Aerodynamic and deposition effects of street trees on PM2.5 concentration: from street to neighborhood scale

Xinlu Lin¹*, Marcelo Chamecki ², Xiping Yu ³

4 Abstract

In this study, large eddy simulation (LES) is adopted to evaluate the aerodynamic and deposition effects of street trees on fine particulate matter (PM2.5) concentration within street canyons. The Extended Nonperiodic Domain LES for Scalar Transport (ENDLESS) is used to allow exploration of vegetation effects at a neighborhood scale (up to 100 canyons) while maintaining a reasonable resolution required to resolve flow patterns within each canyon. We investigate three emission scenarios: (i) only local traffic emissions within the canyon (the first canyon in the urban environment); (ii) only background pollution originating from the upwind canyons; and (iii) a combination of scenarios (i) and (ii). Numerical results show that the presence of trees has different effects on the PM2.5 level within canyons in different emission scenarios and at different spatial scales. At the street scale with only local traffic emissions, aerodynamic effect of trees results in an increase in the concentration near leeward walls and a decrease in the concentration near windward walls, which overwhelms the deposition effect. On the other hand, trees have a negligible impact on the transport of background pollution into the canyon or its distribution within the canyons. The deposition has beneficial effects that only manifest in a considerable way at the neighborhood scale. Finally, the effect of trees on a simple operational urban

¹ Corresponding author, Associate Professor, College of Civil Engineering, Fuzhou University, Fuzhou, China. Email: linxinlu@fzu.edu.cn

² Professor, Department of Atmospheric and Oceanic Sciences, University of California, Los Angeles, Los Angeles, USA

³ Professor, State Key Laboratory of Hydroscience and Engineering, Department of Hydraulic Engineering, Tsinghua University, Beijing, China.

- pollution model (OUPM) is investigated. After modifications for aerodynamic and deposition effect of trees, the predictions of the OUPM show good agreement with LES results.
- 21 **Keywords:** Large Eddy simulation (LES); Pollutant deposition; Street canyon; Urban vegetation;

Elevated concentrations of fine particulate matter (PM2.5) in urban areas are a growing concern

22 Urban pollution model

19

20

23

24

25

26

27

28

29

30

31

32

33

34

35

36

37

38

39

40

41

42

1 Introduction

due to its effect on human health and climate (Pope et al., 2002; Pöschl, 2005). Traffic emissions generally constitute an important source of aerosol precursor gases and primary ultrafine particles in the ambient air (Maricq et al., 1999; Zhu et al., 2002). Under unfavorable meteorological conditions (e.g., weak wind speeds and shallow planetary boundary layers), the interplay of local traffic emissions and regional emissions can result in severe pollution episodes in megacities such as Beijing, China (Zhao et al., 2013; Guo et al., 2014). One possible remediation strategy to help improve the ambient air quality in urban regions is to increase the urban vegetation coverage. This strategy is based on the collection capability of vegetation because it provides large surface areas for the absorption and deposition of gases and particles (Lovett, 1994; Beckett et al., 2000; Freer-Smith et al., 2004; Freer-Smith et al., 2005). Numerous field studies have provided evidence that the increase in vegetation coverage is related to lower particle pollution in urban areas (Cavanagh et al., 2009; Yin et al., 2011; Chen et al., 2015; Irga et al., 2015; Yli-Pelkonen et al., 2017; Chen et al., 2019). In contrast, a few field studies have reported contradictory results showing that urban vegetation such as forests or barriers have an insignificant effect reducing PM concentrations (Setala et al., 2013; Brantley et al., 2014). Particularly, increasing PM2.5 levels were observed within street canyon by Jin et al. (2014). There are two possible reasons for this: (i) vegetation influences airflow via drag forces, which may contribute to the accumulation of PM in specific locations within the urban environment; and (ii) as particle removal by deposition varies widely depending on the characteristics of vegetation, particles, and wind, this effect may not be very efficient at times. The complexity of this problem calls for an accurate assessment of the effects of urban vegetation on PM concentrations in urban environments.

43

44

45

46

47

48

49

50

51

52

53

54

55

56

57

58

59

60

61

62

63

64

65

66

67

68

In recent decades, many studies have been undertaken to investigate the effects of urban vegetation on PM. Janhäll (2015), Abhijith et al. (2017) and Buccolieri et al. (2018) have provided comprehensive reviews. Britter and Hanna (2003) suggests that the flow and dispersion in urban area can be addressed at four scales: regional (up to $100\sim200 \text{ km}$), city (up to $10\sim20 \text{ km}$), neighborhood (up to $1\sim2 \text{ km}$), and street (less than 100~200m). At street scale, the problematic air pollution within street canyon is a research hotspot because of the potentially high traffic volume and poor ventilation conditions. Wind tunnel and computational fluid dynamics (CFD) studies indicate that the aerodynamic effect of vegetation reduces ventilation and circulation and favors increased pollutant concentration within the idealized two-dimensional (2D) canyon, especially on the leeward side (Ries and Eichhorn, 2001; Gromke and Ruck, 2007; Buccolieri et al., 2009; Buccolieri et al., 2009; Gromke and Ruck, 2012; Moonen et al., 2013; Wang et al., 2018). Recently, a few numerical studies sought to consider both aerodynamic and deposition effect. Vos et al. (2013) and Vranckx et al. (2015) found that aerodynamic effect appears to overshadow the pollutant removal capacity of vegetation at single street scale. Meanwhile, Xue and Li (2017) and Santiago et al. (2017) suggested that deposition can also be a major effect both for street canyon geometry and for cube geometry. In city-scale studies, Jeanjean et al. (2016, 2017) argued that the aerodynamic effect is stronger than the deposition effect and highlighted the importance of local meteorology. However, all of these studies are based on Reynolds-averaged Navier-Stokes models and use constant deposition velocity V_d , which is decoupled from local wind velocities. Further, most studies only considered the condition with local traffic emission at street scale. In fact, background pollution can dominate severe air pollution scenarios.

Additionally, although the microscale CFD simulations provide detailed information and help understand the dispersion and deposition process, the computational cost makes it unfeasible for practical applications. Typically, simplified models based on street canyon models or street network

- models are used for operational purposes (Namdeo and Colls, 1996; McHugh et al., 1997; Soulhac et al., 2011). To the best of our knowledge, however, most of them have not considered the effect of trees within streets canyons.
- Therefore, the objectives of this study are:

69

70

71

78

79

80

81

82

83

84

85

86

87

88

- (1) to evaluate the aerodynamic and deposition effect of trees in canyons under different emission
 scenarios;
- 75 (2) to examine the effect of leaf area index (LAI) on the dispersion and deposition at the street and 76 neighborhood scales; and
- 77 (3) to devise a strategy to include the effect of trees in operational urban pollution model (OUPM).
 - To better represent turbulence, the simulations are conducted with large eddy simulation (LES) models. The canonical 2D street canyon is employed, which has been widely adopted to study both ventilation and pollutant dispersion in wind tunnel (Meroney et al., 1996; Pavageau, 1996; Pavageau and Schatzmann, 1999; Brown et al., 2000) and CFD studies (Cui et al., 2004; Wong and Liu, 2013; Michioka et al., 2016; Wang et al., 2018). To evaluate the effect of vegetation on different sources of pollution, we investigated three emission scenarios: (i) only local traffic emissions; (ii) only background
 - The rest of this paper is organized as follows: Section 2 describes the numerical model and simulation set-ups. Model validation is briefly presented in Section 3. The results and discussion are presented in Section 4, and in Section 5, we draw the conclusions.

field pollution originating from upwind canyons; and (iii) a combination of scenarios (i) and (ii).

2 Methodology

- 89 *2.1 LES*
- 90 2.1.1 Flow over street canyon with vegetation
- The LES model together with an immerse boundary method (IBM) is employed to simulate the flow over an urban geometry and a drag force is used to represent the effects of vegetation. For brevity,

only important features of the numerical model are presented here and the readers may refer to Anderson et al. (2015) and Li et al. (2016) for more details on the IBM and Pan et al. (2014) for the canopy model. In the present study, only the neutrally stratified boundary layer is considered, and the turbulence caused by vehicle motion is assumed to be negligible. Under these conditions, the spatially filtered three-dimensional (3D) momentum equation for incompressible air flows is written as

98
$$\frac{\partial \tilde{\mathbf{u}}}{\partial t} + \tilde{\mathbf{u}} \cdot \nabla \tilde{\mathbf{u}} = -\frac{1}{\rho} \nabla \tilde{p} - \nabla \cdot \boldsymbol{\tau} + \mathbf{B} + \mathbf{F}_{d} , \qquad (1)$$

where $\tilde{\mathbf{u}}$ is the filtered velocity, $(1/\rho)\nabla\tilde{p}$ is the filtered pressure gradient force, $\boldsymbol{\tau}$ is the subgrid-scale (SGS) momentum flux, \mathbf{B} is the immersed boundary force representing the effect of solid obstacles immersed in the flow, and \mathbf{F}_d is the additional drag force imposed by the vegetation.

For simplicity, the urban setting is modeled as a sequence of 2D canyons, with the wind blowing perpendicular to the buildings to study the worst ventilation case. The buildings are modeled using a ghost-cell immersed boundary method (Tseng and Ferziger, 2003). The immersed boundary force **B** is zero within the fluid and nonzero inside the buildings (it is adjusted to maintain zero velocity inside the buildings).

The drag force used to represent the effects of the trees on the flow is given by (Shaw and Schumann, 1992; Pan et al., 2014)

$$\mathbf{F}_{d} = -C_{d}(a\mathbf{P}) \cdot (|\tilde{\mathbf{u}}|\tilde{\mathbf{u}}) , \qquad (2)$$

where C_d is the drag coefficient (assumed to be constant in this study), a(z) is the two-sided leaf area density (LAD), and $\mathbf{P} = P_x \mathbf{e}_x \mathbf{e}_x + P_y \mathbf{e}_y \mathbf{e}_y + P_z \mathbf{e}_z \mathbf{e}_z$ is the projection coefficient tensor to project the LAD into streamwise (x), spanwise (y), and vertical (z) directions (here we use a typical drag coefficient $C_d = 0.2$ and identical projections onto the three orthogonal planes given by $P_x = P_y = P_z = 1/3$).

The momentum equations are solved using a pseudo-spectral approach in the horizontal direction and a second-order, centered, finite-difference scheme in the vertical direction. The Lagrangian scale-dependent dynamic Smagorinsky SGS model (Bou-Zeid et al., 2005) is employed to close the equations

and a second-order Adams–Bashforth scheme is used for temporal integration. To reduce the error from
Gibbs phenomenon around the buildings, a cubic interpolation smoothing method is applied before
computing the horizontal spectral derivatives (Li et al., 2016).

2.1.2 Dispersion and deposition of pollutant

120

121

122

123

124

125

The focus of the present work is on exhaust particles from traffic emissions, which are predominantly in the ultrafine range (Maricq et al., 1999; Zhu et al., 2002). At this particle size, the gravitational settling and inertial effects can be neglected; hence, the particles are transported as passive tracers and their diameter only affects the deposition process. The particle concentration is thus governed by the following advection-diffusion equation:

$$\frac{\partial \tilde{C}}{\partial t} + \tilde{\mathbf{u}} \cdot \nabla \tilde{C} = \nabla \cdot \boldsymbol{\pi}^{C} - S_{d} + q_{\text{src}},$$
(3)

where \tilde{C} is the filtered particle concentration [g m⁻³], π^{C} is the SGS concentration flux [g m⁻² s⁻¹] (computed using a dynamic SGS viscosity with a constant SGS Prandtl number, $Pr_{SGS} = 0.4$), q_{src} is the local particle release rate [g m⁻³ s⁻¹], and S_d is the rate of particle deposition on the canopy elements [g m⁻³ s⁻¹]. The sink term can be expressed as

$$S_d = \alpha_g v_d \tilde{C} \quad , \tag{4}$$

where α_g is a geometric factor with a unit of m⁻¹ and includes the effects of leaf density and morphology (here set to a/π), and v_d is the deposition velocity on the vegetation element. Instead of using a single constant deposition velocities in the whole field, a dynamic deposition model is adopted as

$$v_d = |\tilde{\mathbf{u}}| E_D \quad , \tag{5}$$

where E_D is the collection efficiency, formulated as

138
$$E_D = 1.88 \,\mathrm{Re}^{-1/2} \,\mathrm{Sc}^{-2/3} + 2d_p / d_l \quad . \tag{6}$$

Here $\text{Re} = |\tilde{\boldsymbol{u}}| d_1 / v$ is the Reynolds number, $\text{Sc} = v / D_{\text{B}}$ is the Schmidt number, d_{p} is the aerodynamic diameter of particles, d_{l} is the characteristic dimension of the vegetation elements (chosen as 0.001 m), and v is the kinematic viscosity of air. D_{B} is the diffusivity for the particles in the air as a consequence of Brownian motion expressed as

$$D_{\rm B} = C_{\rm C} k_{\rm B} T / \left(3\pi\mu d_{\rm p}\right). \tag{7}$$

Here $k_{\rm B}$ is Boltzmann constant, T is the absolute temperature, μ is the dynamic viscosity of air, and $C_{\rm C}$ is the Cunningham correction factor, which is calculated by

146
$$C_{C} = 1 + \frac{\lambda}{d_{p}} \left[2.514 + 0.8 \exp\left(-0.55 \frac{d_{p}}{\lambda}\right) \right], \tag{8}$$

where λ is the mean free path of air (66 nm at a temperature of 20°C).

The two terms in the right-hand side of Eq. (6) denote the deposition on the foliage corresponding to Brownian diffusion and interception, respectively. Note that the only change compared to the ultrafine particle deposition model developed by Lin et al. (2018) is the inclusion of the second term on the right-hand side of Eq. (6). As we are only interested in particles smaller than 1 µm (in both Aitken and accumulation mode), the effects of impaction and gravitational sedimentation can be neglected (Petroff et al., 2008). The model has been implemented in LES and has been shown to produce mean concentration and turbulent fluxes of ultrafine particles in agreement with observations over a Scots pine forest (Lin et al., 2018).

A finite-volume method (FVM) with the bounded advection scheme SMART (Gaskell and Lau, 1988) is adopted to avoid unphysical oscillations and negative concentrations near localized sources and sinks. To obtain the velocity field needed for the finite-volume discretization (Fig. S1 in the Supplement), the conservative interpolation of Chamecki et al. (2008) is adopted with a modification to account for the buildings (see Supplement for details). In addition, by using FVM instead of the pseudo-spectral approach, the particle concentration does not need to be smoothed inside buildings.

We also adopted the Extended Nonperiodic Domain LES for Scalar Transport (ENDLESS) approach developed by Chen et al. (2016). ENDLESS uses a velocity field simulated in a smaller domain

to simulate a scalar field on a much larger scale (Fig. 1). In this study, the velocity field is simulated over a small number of canyons (i.e., at the street scale) at a fairly high resolution and employed to simulate concentrations plumes at the neighborhood scale (100 canyons). The use of periodic boundary conditions in the velocity field enables recycling of the small domain. In the present application, the scalar fields are extended only in the streamwise direction. The concentration at the downstream boundary in a given domain is used as inflow at the upstream boundary in the next domain, so that the evolution of plumes larger than the velocity field domain can be calculated. Even though ENDLESS produces artificial correlations at distances larger than the velocity field domain, it has been shown that single point statistics are in excellent agreement with the traditional LES approach (Chen et al., 2016; Chen et al., 2018). Technical details of implementation and computational cost, as well as a detailed assessment of the approach are presented in Chen et al. (2016).

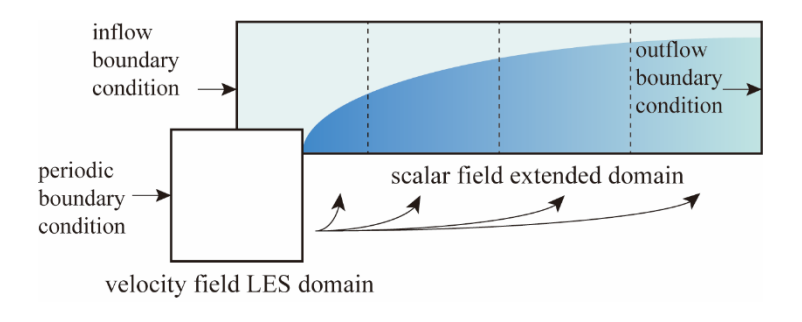
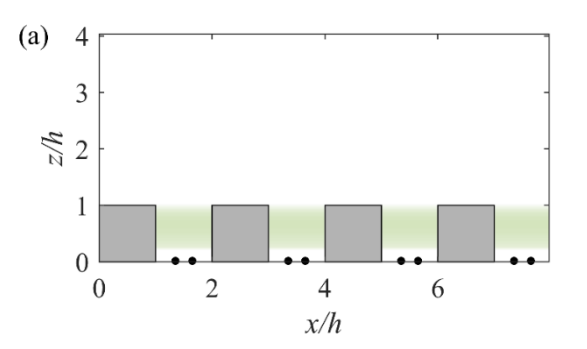


Fig. 1 (Color online) The simple sketch of the ENDLESS framework (in x-z plane).

2.2 Simulation set-up



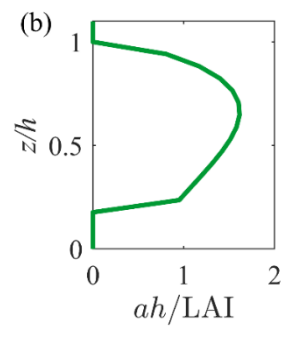


Fig. 2 (Color online) (a) Computation domain for flow field. The gray solid squares, black dots, and green shadow represent the buildings, line traffic sources, and leaf area, respectively; (b) The vertical profile of the

normalized leaf area density (a) normalized by its mean value LAI/h.

182

183

184

185

186

187

188

189

190

191

192

193

194

195

196

197

198

199

200

201

202

203

204

205

206

207

The simulations of flow fields are performed on a box domain of length $L_x \times L_y \times L_z = 8h \times 4h \times 4h$, including four street canyons (Fig. 2a). The height of canyons h is set to 15.5 m and the aspect ratio $h/w_{\rm c}$ is set to 1, where $w_{\rm c}$ is the width of the canyon (equal to the width of the building, $w_{\rm b}$). Thus, the flow within canyons is characterized by "skimming flow" (Oke, 1988), which is adverse for the ventilation and exchange of pollutants. Two line sources with releasing rate q/2 [g m⁻¹s⁻¹] each are placed within canyons to represent the traffic emissions. LAI is the vertical integral of LAD (denoted by a as before). Most LAI of trees is in the range 3–10 (Teske and Thistle, 2004). For example, Norway spruce has an LAI of 10.5 with a height of 8 m, and Bur oak has an LAI of 3.04 with a height of 17.43 m. To test the effect of crown density, seven simulations are performed with different two-sided LAI (0, 0.5, 3, 6, 9, 12, 15). Thus, the range of LAI can cover cases from no vegetation, very sparse, to very dense. For all these simulations, normalized LAD distributions are the same and tend to be homogeneous between $3.5 \text{m} \le z \le h$ (Fig. 2). The LAD below 3.5 m is set as 0 to ensure the open space for vehicles. The effect of trunks is neglected. Although fairly idealized, this setup is fairly representative of many urban regions in China. The flow is driven by a constant pressure gradient of u_{τ}^2/L_z in the streamwise momentum equation, where u_{τ} is a nominal friction velocity scale and is set to 0.45 m/s. A log-law wall model is adopted on the surface of obstacles and at the ground (Anderson et al., 2015). A stress-free condition is applied at the top boundary, and periodic boundary conditions are employed in the horizontal directions. For particle field, exhaust particle number distribution is observed comprising two modes, one with a mean diameter below 30 nm and another with a mean diameter approximately 70 nm (Karjalainen et al., 2014). Even though inertial effects can be neglected, collection efficiency still shows strong dependence on particle diameter (note that $D_{
m B} \propto d_{
m p}^{-1}$ so that the Brownian diffusion term is proportional to $d_p^{2/3}$ while interception increases linearly with d_p). As expected from the reduction in deposition velocity with increasing particle size in this range (see Fig. S3 in Supplement), $d_p = 15 \text{ nm}$ is selected for its high collection efficiency. Control cases with $v_d = 0$ are conducted to evaluate the

aerodynamic effect. These two cases bound the behavior of most particle sizes in the range of interest. The concentration at the domain inlet was set to zero and an open boundary condition was adopted at the outlet. Because the deposition on the vegetation is more than 10 times more efficient than on the building surfaces (Roupsard et al., 2013), the deposition on the building surfaces is neglected in this study. Hence, the no-flux condition was used on all surfaces of the canyons and the ground. For the top boundary, an impermeable boundary condition is used because the vertical velocity is set to w = 0 at the top and the SGS diffusivity also vanishes. To study the development of plume and assess the deposition effect at the neighborhood scale, the concentration domain was extended in the streamwise direction to 25 L_x employing the ENDLESS approach (Fig. 3). In all simulations, clean air conditions were specified for the inflow concentration boundary condition. Thus, air pollution within the first canyon was only caused by local emissions while air pollution within the downwind canyons were also affected by transport from upwind canyons (this transport of pollution from upwind canyons is referred to as "background pollution", even though this is not the most common use of this terminology). In this study, we are interested in three emission scenarios: (i) only local traffic emissions; (ii) only background field pollution originating from upwind canyons; (iii) a combination of scenarios (i) and (ii). The air quality within the first canyon and the 97th canyon can be a good proxy for scenarios (i) and (iii). Hereafter, these two canyons are referred to as CA1 and CA3 (Fig. 3a). To evaluate scenario (ii), we ran additional simulations with only one scalar domain and without local emissions (Fig. 3b). The time series of concentration of the x-z plane between Domain 24 and Domain 25 in ENDLESS simulation with LAI = 0 were recorded and then used as the inflow boundary condition for the Background simulation. Thus, concentrations in the Background simulation are all caused by upwind pollution. The first canyon near the inflow boundary in the

208

209

210

211

212

213

214

215

216

217

218

219

220

221

222

223

224

225

226

227

228

229

230

Background simulation is referred to as CA2 (Fig. 3b). It should be stressed that all the inflow pollution

of the Background simulation is the same in different LAI cases, whereas the background pollution in CA3 will be affected by different LAI in upwind canyons.

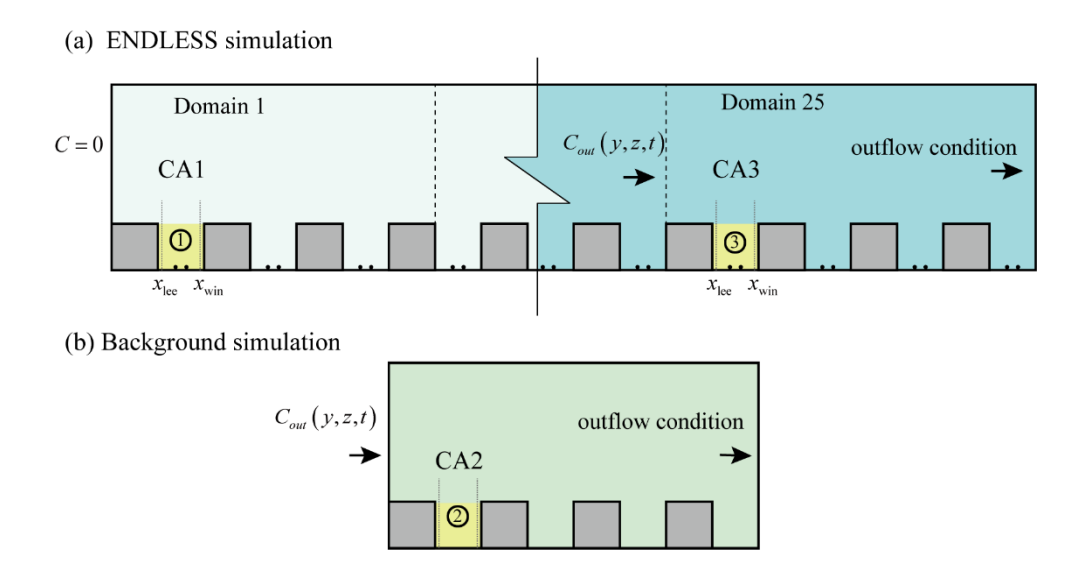


Fig. 3 The canyons representing three emission scenarios: (i) only local traffic emissions (CA1); (ii) only background pollution (CA2); (iii) a combination of (i) and (ii) (CA3). The dotted lines represent the leeward and windward *y-z* planes within canyons, which are used for latter analysis.

All the simulations are performed with a constant grid spacing of $\Delta = h/17$. Additionally, a sensitivity test with double resolution showed that the resolution adopted here is enough to capture the main characteristics of flow and concentration fields.

2.3 Averaging and notation

Simulations were performed for a period of 60T ($T = h/u_{\tau}$) for the flow to achieve statistically steady state, and then another 160T with the pollution sources. The second half of the pollution period, when the plume is already in a statistical steady state, was used for data collection.

Given the 2D geometry, all variables of interest (generically represented by X(x,y,z,t)) are averaged in time and in the spanwise (cross-flow) direction, which is indicated as $\overline{X}(x,z)$. For specific analysis, further averages in the streamwise direction are represented by $\langle \overline{X} \rangle_x(z)$, while averages over

247 the entire canyon volume are denoted by $\langle \overline{X} \rangle_{\rm C}$ and defined as

$$\left\langle \bar{X} \right\rangle_{\rm C} = \frac{\iint_{\Omega} \bar{X} dx dz}{h w_{\rm c}} \quad , \tag{9}$$

- where Ω is the region within the canyon in x-z plane. In addition, $\bar{X}_{lee}(z)$ and $\bar{X}_{win}(z)$ represent
- 250 the temporal and spanwise average variable at $x = x_{lee}$ and $x = x_{win}$, respectively (which is 1.5 Δ outside
- 251 the walls to avoid the influence of the walls and corners, see Fig. 3).
- 252 Finally, we define three normalized canyon-averaged bulk variables: the canyon-averaged
- normalized concentration $\langle \bar{C}^* \rangle_C$; the normalized spatial concentration variance σ_C^* ; and the canyon-
- 254 averaged normalized deposition velocity V_d^* :

$$\left\langle \bar{C}^* \right\rangle_{\rm C} = \left\langle \frac{\bar{C}u_{\rm r}h}{q} \right\rangle_{\rm C} , \qquad (10)$$

$$\sigma_C^{*2} = \frac{\sigma_C^2}{\left\langle \overline{C}^* \right\rangle_C^2} , \qquad (11)$$

$$V_d^* = \frac{h w_c \left\langle \overline{S}_d \right\rangle_C}{q \left\langle \overline{C}^* \right\rangle_C},\tag{12}$$

- where $\sigma_{\rm C}^2 = \sum \left(\overline{C}^*(x,z) \left\langle \overline{C}^* \right\rangle_{\rm C} \right)^2 / N_{\rm C}$, $N_{\rm C}$ is the number of nodes within the canyon. The variation
- of these four dimensionless variables with the canyon number (n) will be discussed in a later section.

261 2.4 Validation

260

262

263

264

265

266

The code for the LES model has been validated using wind tunnel measurements for turbulence around 3D cubes (Anderson et al., 2015; Li et al., 2016), and validated using field measurements for ultrafine particle deposition (Lin et al., 2018). To evaluate the model accuracy for turbulence and pollutant dispersion within and above continuous street canyons, we simulated a configuration used in several wind tunnel measurements (Meroney et al., 1996; Pavageau, 1996; Pavageau and Schatzmann,

1999; Brown et al., 2000). The configuration was identical to the 2D street canyons with a unity aspect ratio, while the height of ribs is 0.06 m in the wind tunnel experiments. Four simulations with three types of computational domain $(4h \times 2h \times 4h, 8h \times 4h \times 4h, and 8h \times 4h \times 8h)$ and two types of mesh $(\Delta = h/17 \text{ and } \Delta = h/31)$ were conducted. For brevity, more details of the validation set-up and the comparison of results are shown in the Supplement. The mean flow and turbulence statistics of all three simulations agree well with wind tunnel measurements. Results indicate that the case with computational domain of $4h \times 2h \times 4h$ and resolution of $\Delta = h/17$ (WT424-17) can provide an accurate prediction of flow statistics within and near canopy. Even though fine LES results show better agreement with measurements, WT424-17 can reproduce most of the main features of the concentration field. It should also be noted that a resolution of h/16 is widely used in LES simulations of flow over urban-like topographies (Boppana et al., 2014; Anderson et al., 2015; Li and Wang, 2018), and is considered adequate to resolve the main characteristics of the flow and scalar plume in the present simulation. To test the sensitivity of results to the computational domain in ENDLESS scenarios, we run three cases with different velocity domains to mimic the dispersion of plume (details can be found in Supplement). Results show that concentration fields using ENDLESS with a velocity domain of $8h \times 4h \times 4h$ agree well with those obtained from a traditional LES simulation with a velocity domain of $20h \times 10h \times 4h$ (Fig. S8). Considering the computational cost to extend the scalar domain to reach a neighborhood scale using ENDLESS, we adopt the computational domain of $8h \times 4h \times 4h$ and resolution of $\Delta = h/17$ in this study.

3 Results and Discussion

267

268

269

270

271

272

273

274

275

276

277

278

279

280

281

282

283

284

285

286

287

288

289

290

3.1 Effects of trees on canyon particle concentration with different emission conditions

Before evaluating the effects of trees on canyon particle concentration, we first explore how the trees affect the flow within canyons. With an aspect ratio of 1, the skimming flow (as noted by Oke (1988)) drives an isolated clockwise mean flow vortex within the canyon in the control case. The trees,

treated as a sink of momentum, strongly weaken the vortex and reduce the circulation within the canyon (Fig. 4).



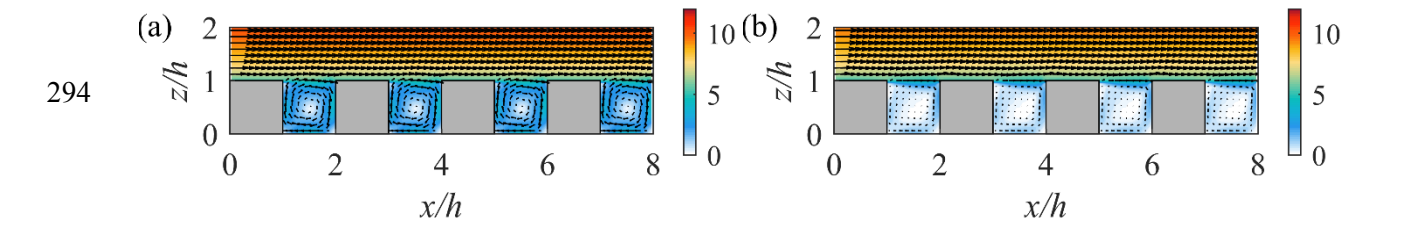


Fig. 4 (Color online) Mean wind vectors and magnitude of normalized velocity in the street canyon for simulation (a) LAI 0 and (b) LAI 6.

The profiles of horizontally averaged turbulence statistics are presented in Fig. 5. Strong reduction in the mean flow and turbulence intensity can be observed within the canyon due to the increase in the LAI. The air exchange rate $\text{AER} = \int_{\Gamma} \left(\overline{w}_+ \big|_{\text{roof}} + 1/2 \, \overline{w^+ w^-} \big|_{\text{roof}} \right) \mathrm{d}\Gamma$ at the roof level is usually employed to represent the rate of removal of airflow in street canyons (Xie et al., 2006; Cheng et al., 2008). Similarly, vertical air exchange rate $\text{VAER} = \left< |\overline{w}| + \sigma_w \right>_x / (2u_\tau)$ represents ventilation within and above canyons. Due to the mean flow vortex, the mean vertical motion contributes a large portion of the ventilation within the canyon, while above the roof, the vertical ventilation is controlled by turbulence (Fig. 5c). Although the VAER at the roof level shows very weak reduction with the variation of LAI, VAER within the canyon strongly diminishes with increasing LAI. This suggests that vegetation might still worsen pedestrian-level air quality.

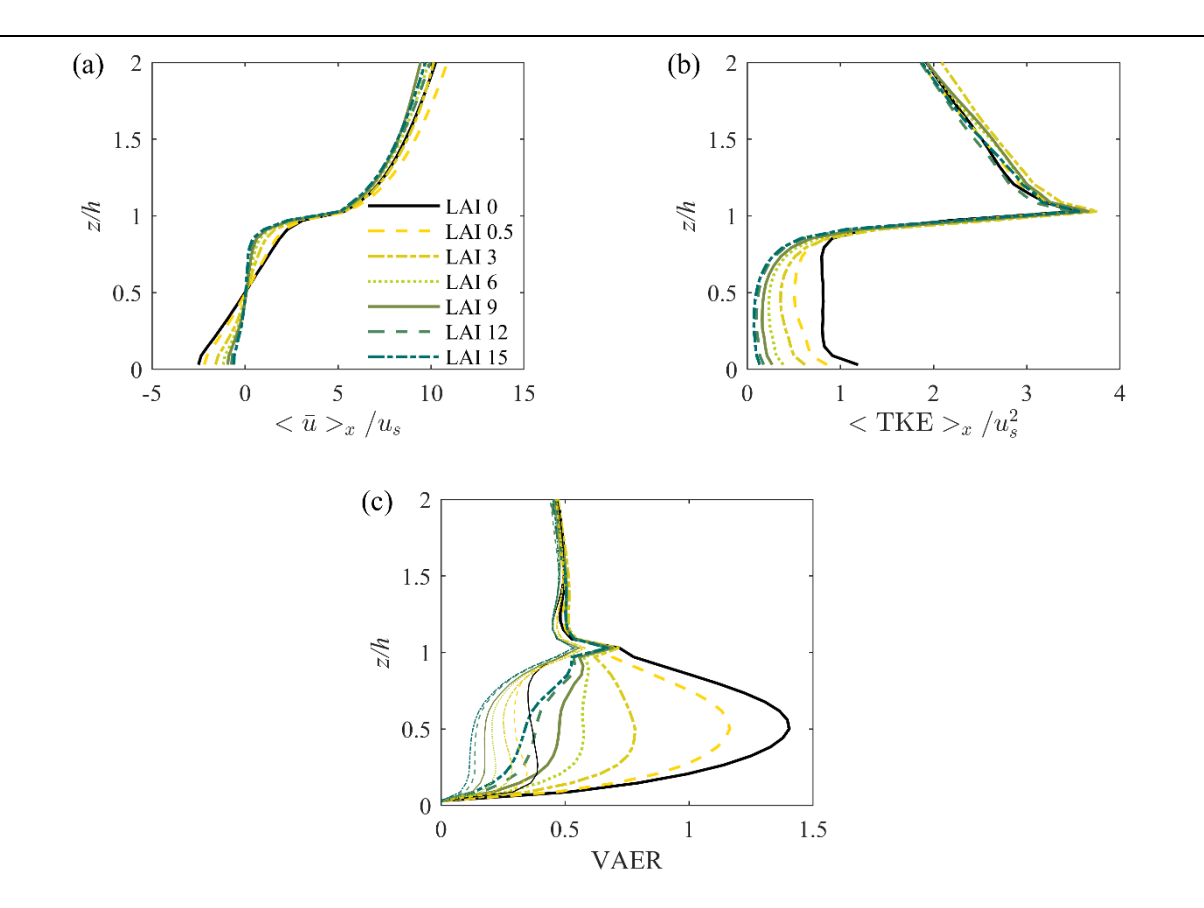


Fig. 5 (Color online) Vertical profiles of normalized (a) mean streamwise velocity, (b) turbulent kinetic energy, and (c) vertical air exchange rate. The finer lines in (c) represent the standard deviation part $\langle \sigma_w \rangle_x / (2u_s)$.

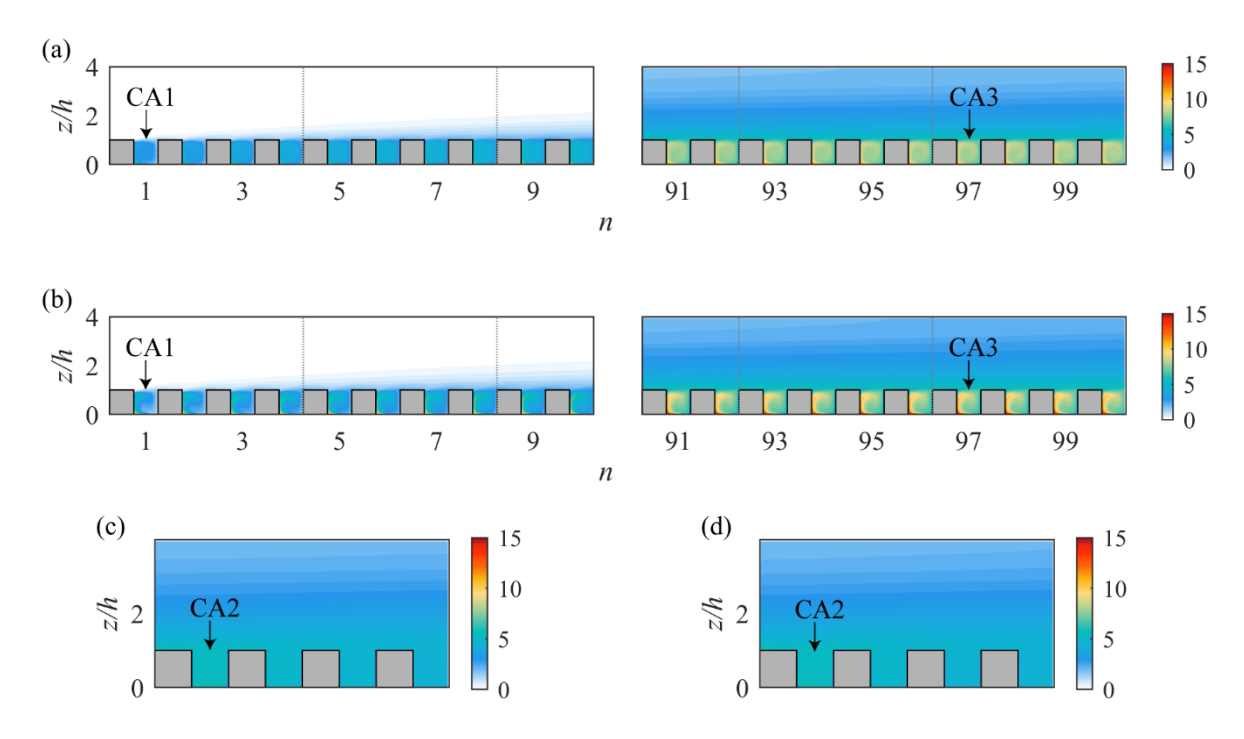


Fig. 6 (Color online) The particle concentration distribution without deposition effect for ENDLESS simulations
(a) LAI 0 and (b) LAI 6 (without deposition) and Background simulations (c) LAI 0 and (d) LAI 6 (without

309

310

311 deposition).

Fig. 6 shows the particle concentration distribution of ENDLESS simulations and Background simulations. Although the height of the computational domain (62 m) is lower than the typical height of atmospheric boundary layer (between 100 and 1000 m), our simulations represent a rough approximation of the concentration build-up in an urban environment. Note that the aerodynamic effect of trees produces a more heterogeneous distribution of concentration in the presence of local sources (Fig. 6 a, b), while no difference can be found in Background simulations (Fig. 6 c, d).

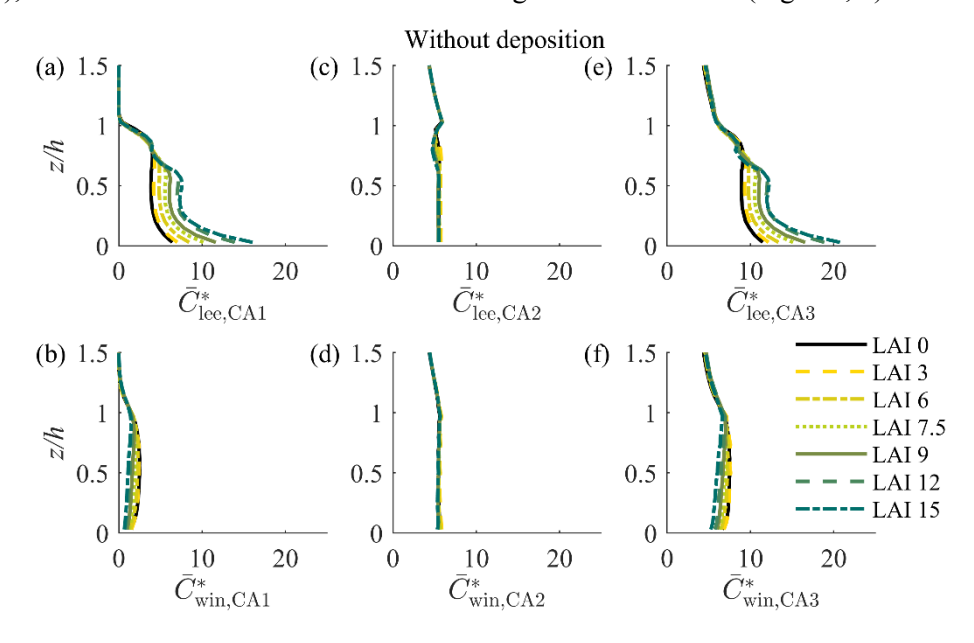
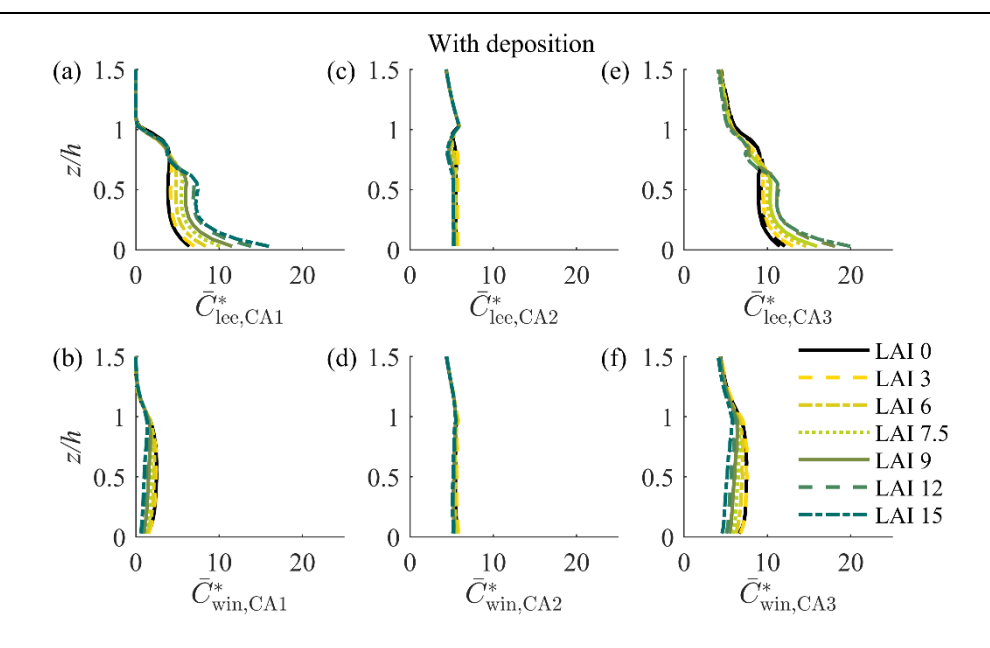


Fig. 7 (Color online) Vertical profiles of normalized mean concentrations on the leeward and windward side in CA1 (a and b), CA2 (c and d), and CA3 (e and f) canyon (only considering aerodynamic effect).



321

322

323

324

325

326

327

328

329

330

331

332

333

334

335

336

337

338

Fig. 8 (Color online) Similar to Fig. 7, but deposition effect is included.

Fig. 7 and Fig. 8 show the profiles of normalized mean concentration near the leeward and windward wall excluding and including deposition effect, respectively. When deposition effect is excluded, increases in canopy LAI lead to considerable increase in concentration near the leeward wall and decrease near the windward wall under the local emission condition (Fig. 7 a, b). This is a direct consequence of the weakening of the mean circulation inside the canyon (Fig. 4) and is in agreement with wind tunnel measurements (Gromke and Ruck, 2007) and other numerical simulations (Salim et al., 2011; Xue and Li, 2017). In scenario CA2 (Fig. 7 c, d), little difference can be observed between the leeward and windward side concentrations, indicating that the background concentration has a fairly uniform impact on concentrations within the canyon. With the increase in LAI, the negligible reduction of concentrations within CA2 suggests that the aerodynamic effect of trees can be neglected for background pollution at street scale. Additionally, the concentration distribution suggests that the background concentration above the canyon is a good proxy for concentrations everywhere in the canyon in the absence of local sources. As expected, the CA3 cases are almost equivalent to the combination of CA1 and CA2 cases. It is noteworthy that the results for scenarios CA1 and CA2 are general, while the scenario CA3 implies a specific combination between local and background sources of pollution that, in our case, is valid only for the 97th canyon. In this specific case, the concentrations in the leeward wall are dominated by local sources, while most of the contribution to concentrations in the windward wall originates from the background. We expect that for canyons with less upwind pollution (e.g., 10th or 20th), both walls will be locally dominated, while further downwind background levels would dominate the entire canyon.

Negligible difference can be observed between Fig. 7 (a)–(d) and Fig. 8 (a)–(d), indicating that deposition effect has limited impact at a street scale whenever the local traffic (CA1) or background pollutant (CA2) is considered. On comparing Fig. 8 (e)–(f) with Fig. 7 (e)–(f), weak reduction of concentration in both leeward and windward side can be observed when deposition effect is included in CA3. The background concentrations in Fig. 8 are impacted by trees in upwind canyons in CA3 cases, while they are the same in all CA2 cases. An increase in LAI implies an increase in deposition and a slower increase in background levels with the number of canyons. This effect is clearly seen on the concentrations above the canyon in Fig. 8. (e), (f), where a reduction in concentration with increasing LAI can be observed.

To show the effect of trees more quantitatively and intuitively, the canyon-average concentrations $\langle \bar{C}^* \rangle_{C}$ are normalized by the values of the control cases (LAI = 0) in Fig. 9. The deposition mechanism has a positive effect on the average air quality for all the three scenarios (solid symbols versus open symbols). This effect is most noticeable in CA3 because the trees have a considerable impact in reducing the build-up of background pollution. As an overall net negative effect, the aerodynamic effect is very pronounced for the local source (CA1). The aerodynamic effect of vegetation is negligible for the background pollution (CA2). Because CA2 has a constant background concentration (i.e., not sensitive to LAI), it can be interpreted as an assessment of the entrainment of background pollution into the canyon. The results presented here show that the presence of trees has only a very small impact on this entrainment.

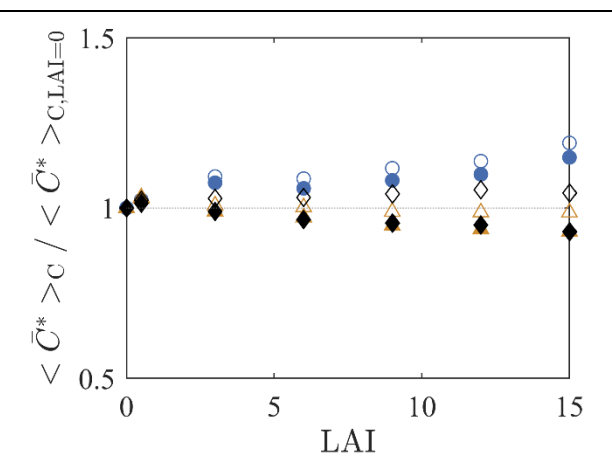


Fig. 9 (Color online) The relative change in the canyon-averaged normalized concentrations for CA1 (blue circles), CA2 (orange triangles), and CA3 (black diamonds). Solid and open symbols represent results with and without deposition, respectively.

When analyzing scenario CA3, one needs to keep in mind that this includes the contribution of both local and background pollution, and that the relative contributions change with the number of upwind canyons. Therefore, results are valid for the set-up with 100 canyons, and conclusions would likely be different with a considerably different number of canyons, e.g., 10 or 1000. For the present conditions, in general, there is a modest improvement in air quality when deposition is included and a comparable deterioration of air quality in the absence of deposition (e.g., particle sizes for which the deposition process is not very efficient).

3.2 Effects of trees on dispersion and deposition at neighborhood scale

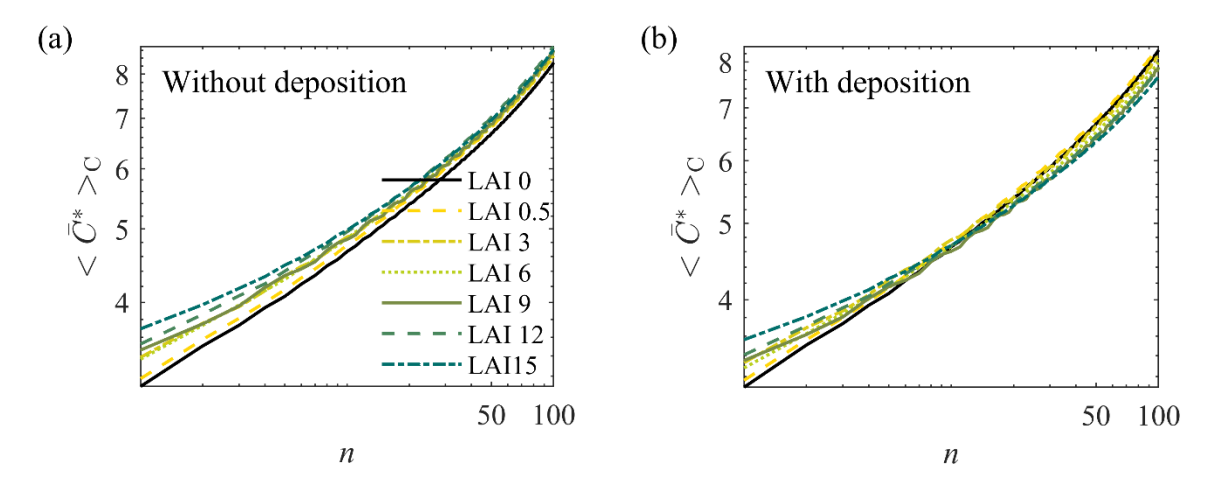


Fig. 10 (Color online) Increase in canyon-averaged normalized concentration with the number of canyons in

ENDLESS simulations: (a) without deposition and (b) with deposition.

According to the discussion in Section 3.1, when only considering the aerodynamic and deposition effect, the presence of trees is harmful to canyon average air quality with local emissions and shows negligible benefit with the same background pollutant. At the neighborhood scale, however, the build-up of deposition effect of trees within canyons can contribute to cleaner air in the downwind area. Fig. 10 shows the development of canyon-averaged concentration $\langle \bar{C}^* \rangle_C$ as a function of canyon number n (n can also be interpreted as the distance from the upwind edge of the urban area, where air is assumed to be unpolluted). The case LAI = 0 serves as a reference, showing the increase in average concentrations with distance from the edge promoted by the accumulation of the pollution in the form of an increasing background concentration. Increasing LAI has a negative effect on the local emissions, reducing ventilation and trapping more pollutants within the canyon. This is clear in the large increase in concentrations in the first canyons, where pollution is dominated by local sources. In the absence of deposition (Fig. 10a), all the different LAI cases approach the no LAI case as distance from the urban edge increases. This is because the background pollution becomes the dominant contribution and the reduced ventilation becomes unimportant. The denser the vegetation, the farther from the edge this convergence occurs, as denser vegetation increases the importance of local pollution sources.

When deposition is included (Fig. 10b), an interesting change in behavior is observed. The first canyons still have greatly enlarged concentrations due to reduced ventilation. However, the curves for different LAIs cross the LAI = 0 case, which means that the inclusion of vegetation has a beneficial effect on air quality. This happens because deposition reduces the rate of increase of the background pollution, which eventually becomes the dominant contribution. Sensitivity simulations with a smaller friction velocity ($u_{\tau} = 0.2 \text{ m/s}$, not shown here) show that the transition point from aerodynamic-dominated effects to deposition-dominated effects (i.e., from concentration enhancement to concentration reduction by trees) moves closer to the city edge. Thus, while this transition is expected to occur for most wind conditions, the precise location will vary depending on wind speed.

Next, the normalized canyon-average concentration variances $\sigma^{*2}_{\ C}$ and deposition velocities V_d^*

are shown in Fig. 11. The former can be used to represent the extent of mixing or homogeneity of pollutant concentration. Increasing LAI considerably increases the heterogeneity of the concentration distribution due to reduced mixing within the canyon. This implies higher localized concentrations near the leeward wall and reduced concentrations near the windward wall. However, with an increase in the distance from the urban edge, background pollution contribution becomes more important and the distribution of concentration within the canyon becomes more homogeneous.

It is also interesting to note that V_d^* is not very sensitive to the concentration distribution (Fig. 11b), especially when LAI is small. The reason may be related to the nearly uniform distribution of the LAD in the canyon in our simulations. When LAI is very large, smaller V_d^* in the first canyon can be observed compared to V_d^* in downwind canyons. This is further discussed in the next section.

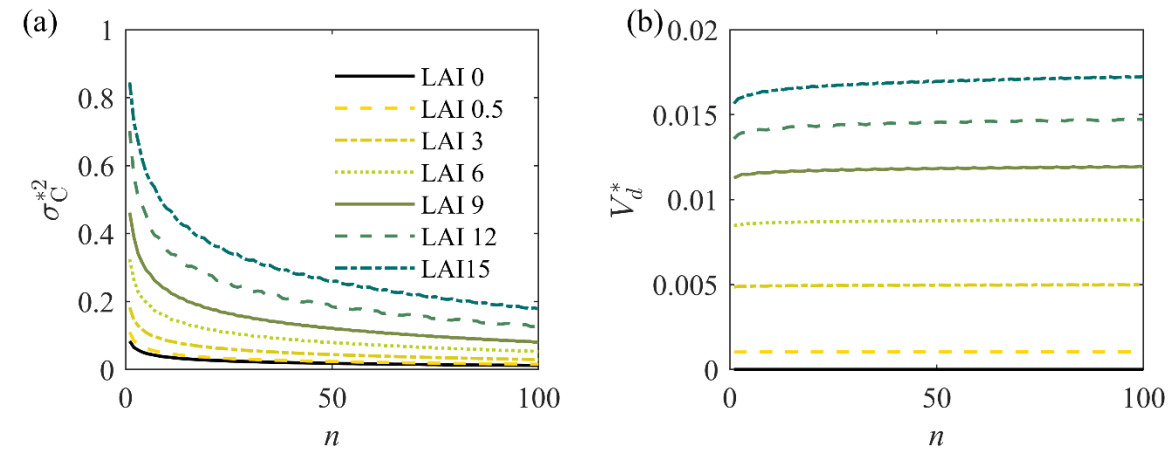


Fig. 11 (Color online) (a) Normalized spatial variance of mean concentration within canyon; (b) normalized deposition velocities.

3.3 Representing effects of vegetation in operational urban pollution models

The results and discussions in the last section imply that urban vegetation plays different roles at different spatial scales. For urban planners, designing or managing urban vegetation requires an accurate evaluation of the effect of trees. Nevertheless, using CFD model to predict air quality and assess the effect of trees at the city scale is always difficult because of the computational cost. Thus, operational or "fast responding" models like ADMS-Urban (McHugh et al., 1997; Carruthers et al., 2000; Righi et al., 2009) or SIRINE (Soulhac et al., 2011; Soulhac et al., 2012; Salem et al., 2015) play an important

role in practical applications. However, few of these models have considered the aerodynamic and deposition effect of urban vegetation. On the other hand, assessment of deposition on vegetation at city scale also requires concentration data, e.g., i -TREE model (Hirabayashi et al., 2012). In this study, we present an investigation of the effects of vegetation on the operational urban pollution model (OUPM) using LES result.

Some key features of the OUPM are: (1) the urban boundary layer is decomposed into the external atmosphere and urban canopy; (2) the external flow is always modeled as boundary layer flow based on Monin–Obukhov similarity theory and dispersion is represented by a Gaussian plume model; and (3) the urban canopy is treated by simplified street canyon model, and the concentration is usually assumed uniform within the canyon. According to the two-domain assumption, the exchange of pollutants between the external atmosphere and street canyon is crucial to a careful model.

In this section, we use the ENDLESS results to develop an approach to incorporate the effect of trees into operational models. First, we consider the cases without trees.

The concentration in an urban canopy can be assumed to consist of two parts, i.e., from local emissions within canyon and external background concentration:

$$\langle \overline{C}^* \rangle_{C} = \langle \overline{C}_{L}^* \rangle_{C} + \langle \overline{C}_{B}^* \rangle_{C} , \qquad (13)$$

where $\langle \bar{C}_L^* \rangle_C$ is the part originating from the local emissions and $\langle \bar{C}_B^* \rangle_C$ is the part originating from the background concentration. As noted in Section 2, the asterisk denotes the normalized process, the angle bracket denotes a spatial averaging process, where the subscript C refers to canyon averaging. For brevity, the overbar denoting the averaging operator in time and the spanwise (cross-flow) direction is omitted in the latter part. Various factors affect the value of $\langle C_L^* \rangle_C$, such as the specific placement and emission rate of local sources, turbulence intensity, geometry of buildings, aspect ratio of canyon, location, and density of trees, and particle size. As it is not the objective of this study to formulate $\langle C_L^* \rangle_C$, we assume $\langle C_L^* \rangle_C$ is known for all LAI cases, which is equal to the concentration in CA1 denoted by $\langle C^* \rangle_C$ (1) (see Fig. 12a).

For $\langle C_{\rm B}^* \rangle_{\rm C}$, it is determined by the background concentration and the flow statistics. As the flow statistics are the same for all canyons in our simulations, the variance of $\langle C_{\rm B}^* \rangle_{\rm C}$ with distance only depends on the background concentration. According to Eq. (13) and the assumption of $\langle C_{\rm L}^* \rangle_{\rm C}$, $\langle C_{\rm B}^* \rangle_{\rm C}$ can be expressed as a function of canyon number (n), and can be obtained by

$$\left\langle C_{\mathrm{B}}^{*}\right\rangle_{C}(n) = \left\langle C^{*}\right\rangle_{C}(n) - \left\langle C^{*}\right\rangle_{C}(1). \tag{14}$$

- To relate $\langle C_{\rm B}^* \rangle_{\rm C}$ to the background concentration, we define the mean normalized concentration above the canyon $C_{\rm R}^*(n)$ as an indicator of background concentration as
- $\left\langle C^{*}\right\rangle_{R}(n) = \frac{\int_{z=h}^{z=1.18h} \int_{(n-1)l+w_{b}}^{nl} C^{*}(x,z) dxdz}{0.2hw_{b}}, \qquad (15)$
- where *n* is the *n*th canyon, and *l* is the sum of the width of building and canyon ($l = w_b + w_c = 2w_b$). Note that this concentration is the average over a layer of depth 3/17 h ($\approx 0.18h$) above the canyon n.
- As local emissions also contribute to the concentration above canyons, we can quantify this by using $\langle C^* \rangle_R$ (1) as a reference for the effects of local emissions, and remove this "local contribution" from the total concentration for any other canyon. Thus, we define the net normalized background concentration $\langle C_B^* \rangle_R$ (shown in Fig. 12b) as

$$\left\langle C_{\mathrm{B}}^{*}\right\rangle_{\mathrm{R}}\left(n\right) = \left\langle C^{*}\right\rangle_{\mathrm{R}}\left(n\right) - \left\langle C^{*}\right\rangle_{\mathrm{R}}\left(1\right). \tag{16}$$

- It can be observed in Fig. 13 that $\langle C_{\rm B}^* \rangle_{\rm R}$ nearly converges with different LAI when the deposition effect is excluded, while the increase in LAI generally contributes to a lower $\langle C_{\rm B}^* \rangle_{\rm R}$ in far downwind areas when including the deposition effect.
 - According to the simulation set-ups, $\left\langle C_{\rm B}^* \right\rangle_{\rm R}(n)$ can also be broken down into the accumulation of the dispersion of upwind emissions. Defining $\left\langle C_{\rm I}^* \right\rangle_{\rm R}(n)$ as the normalized background concentration at canyon n resulting from the emissions from the first canyon (see Fig. 12c), $\left\langle C_{\rm B}^* \right\rangle_{\rm R}(n)$ can be calculated as

$$\left\langle C_{\rm B}^* \right\rangle_{\rm R} \left(n \right) = \begin{cases} 0, & n = 1 \\ \sum_{i=2}^n \left\langle C_1^* \right\rangle_{\rm R} \left(i \right), & n > 1 \end{cases}$$
 (17)

467 Thus, $\left\langle C_{1}^{*}\right\rangle_{\mathbb{R}}(n)$ can be obtained from LES results as

$$\left\langle C_{1}^{*}\right\rangle_{R}\left(n\right) = \left\langle C_{B}^{*}\right\rangle_{R}\left(n\right) - \left\langle C_{B}^{*}\right\rangle_{R}\left(n-1\right), \ n > 1 \quad . \tag{18}$$

469

470

473

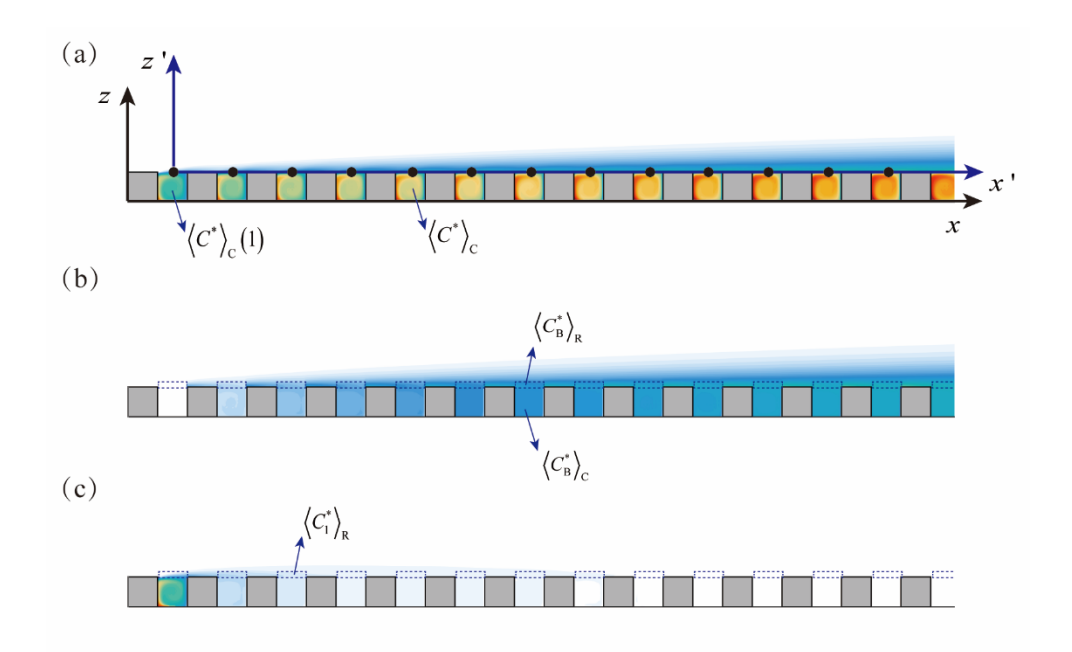


Fig. 12 (Color online) The schematic diagram of (a) plume calculated by LES, (b) accumulated background concentration $\left\langle C_{\rm B}^* \right\rangle_{\rm R}$, and (c) background concentration resulting from the first canyon $\left\langle C_{\rm I}^* \right\rangle_{\rm R}$.

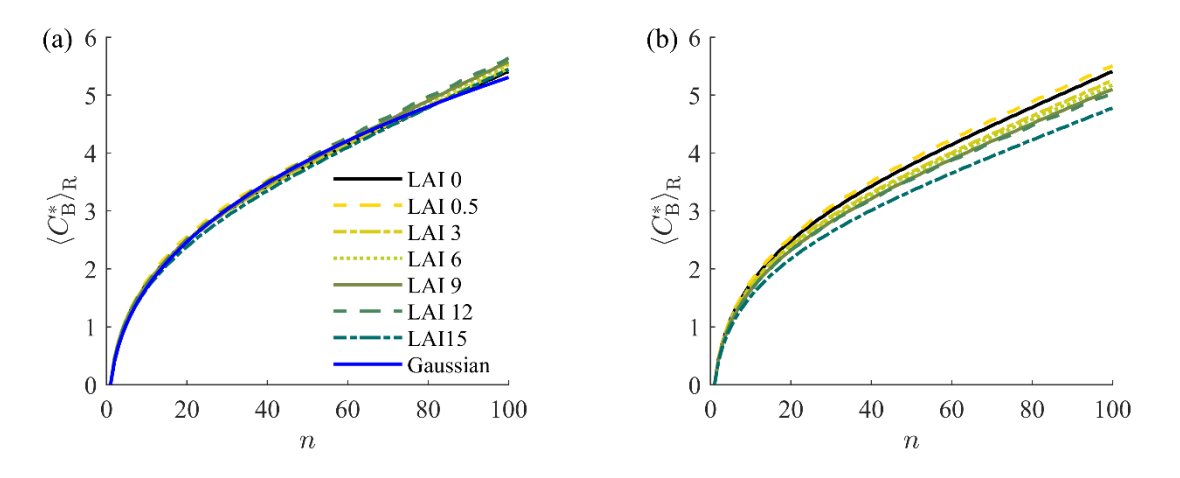


Fig. 13 (Color online) The net normalized background concentration: (a) without deposition and (b) with

474 deposition.

As the dispersion of pollutants above the canopy is commonly modeled by a Gaussian plume model, we assume $\langle C_1^* \rangle_R(n)$ can be approximated by the Gaussian diffusion function for a line source. Here, we define another coordinate system, x'-z', as seen in Fig. 12 (a), and assume that emissions from the first canyon can be approximated as a line source at x'=0,z'=0, which contributes to a concentration field $C_1(x',z')$. Thus, $C_1(x',z')$ can be modeled as

$$C_1(x',z') = \frac{2q}{\sqrt{2\pi}\overline{u}\sigma_z} \exp\left(-\frac{z'^2}{2\sigma_z^2}\right) , \qquad (19)$$

where q is the emission rate, σ_z is the dispersion coefficient (which is a function of x, can be simply modeled as ax^b in neutral stratification, where a and b are empirical parameters), and \overline{u} is the mean wind velocity. According to the normalizing process shown in Eq. (10), we assume $\langle C_1^* \rangle_R(n)$ can be approximated by the normalized concentration in the center point along the roof (i.e., $C_1(2(n-1)w_b, 0)u_rh/q$) of nth canyon, so it can be simplified to:

$$\left\langle C_{1}^{*}\right\rangle_{R}\left(n\right) = \frac{\sqrt{2/\pi}}{\overline{u}^{*}\sigma_{z}^{*}} \quad . \tag{20}$$

Here, $\bar{u}^* = \bar{u}/u_r$, where $\bar{u} = U_s$ and U_s is the average streamwise velocity at height $1 < z/h \le 1.5$ (which is about 7.0 m/s). $\sigma_z^* = \sigma_z/h$ is the modified vertical dispersion coefficient, which can be modeled as $\sigma_z^* = A(n-1)^b$. Therefore, A = 0.28 and b = 0.62 are determined by fitting the approximation to the LES results (LAI 0 case). The value of A depends on the scaling and is difficult to compare with other studies. The value of b is close to another LES simulation conducted by Wong and Liu (2013), which is 0.671 for canyons with an aspect ratio of 1. The difference may arise from the difference of emission set-up and computational domain. It is clear that A and b are usually determined by the turbulence of boundary layer. However, because this study is not designed for a realistic boundary layer, we do not intend to discuss the effect of vegetation on these two parameters. Future research is needed to extend this study to a more realistic urban boundary layer. Using the Gaussian plume model,

 $\left\langle C_{\rm B}^* \right\rangle_{\rm R}(n)$ can be calculated using Eq. (17), which shows good agreement with the LES results (Fig. 498 13a)

In the ENDLESS scenario, concentration within the canyon resulting from background pollution $\left\langle C_{\rm B}^* \right\rangle_{\rm C}(n)$ is not exactly equal to $\left\langle C_{\rm B}^* \right\rangle_{\rm R}(n)$ due to the heterogeneity. However, the relationship between $\left\langle C_{\rm B}^* \right\rangle_{\rm C}(n)$ and $\left\langle C_{\rm B}^* \right\rangle_{\rm R}(n)$ is approximately linear with the variation of distance for all cases (Fig. S9 in Supplement). This suggests a simple model of transport of background pollution into the canyon expressed as

$$\left\langle C_{\rm B}^* \right\rangle_{\rm C}(n) = \operatorname{ER} \left\langle C_{\rm B}^* \right\rangle_{\rm R}(n) , \qquad (21)$$

where ER is an exchange rate obtained from the LES results using a linear fit. When the effect of vegetation is excluded, the ER is approximately 0.95 (Fig. 14a).

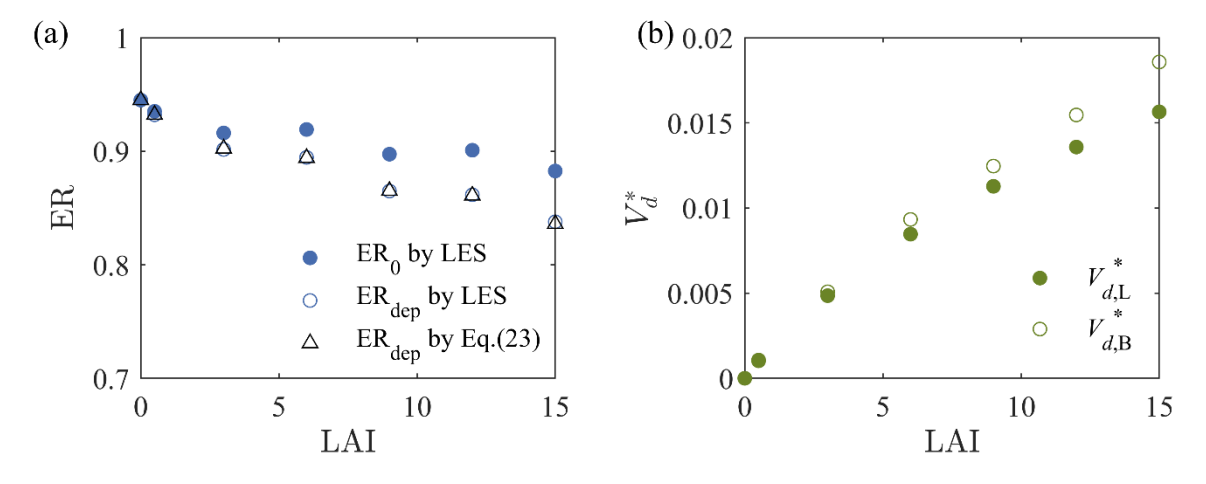


Fig. 14 (Color online) The variation of (a) exchange rate (solid circles and open circle represent ER_0 and ER_{dep} calculated by fitting LES results, open triangles represent ER_{dep} calculated by Eq. 23) and (b) normalized canyon-averaged deposition velocity with the change in LAI (solid circles represent condition with local emission, and open circles and open triangles represent condition with background concentration calculated by ENDLESS simulations or Background simulations).

So far, if $\langle C_L^* \rangle_C$, the emission rate q, the exchange rate ER and the flow features (\bar{u} , dispersion coefficients A and b) are determined, the canyon-averaged concentration can be calculated using the operational dispersion model. Here we defined the relative error between OUPM and LES results:

$$RE = \left(\left\langle C^* \right\rangle_{C} \Big|_{OIIPM} - \left\langle C^* \right\rangle_{C} \Big|_{IES} \right) \times 100\%. \tag{22}$$

Fig. 15a shows that the present OUPM can well predict the concentration without trees. However, if trees are included, the discrepancies between results by the present operational model and LES simulations become apparent. Thus, further modifications need to be made. First, we considered the aerodynamic effect of trees in the operational model. According to our LES results, increase in the crown density of trees contributes to a redistribution of particle concentration and an overall increase of $\langle C_{\rm L}^* \rangle_{\rm C}$ within canyons (Fig. 9). For instance, $\langle C_{\rm L}^* \rangle_{\rm C}$ with all-sided LAI 12 is 13% larger than that without trees. Except for $\langle C_{\rm L}^* \rangle_{\rm C}$, ER values reduces from 0.9451 to 0.8826 when LAI increases from 0 to 15. This may be due to the increase in the heterogeneity of the concentration. In fact, vegetation should also affect the turbulence in the outer layer to influence the dispersion coefficients. For instance, Giometto et al. (2017) showed that vegetation can increase the roughness length and displacement height in a boundary layer-scale study. In ENDLESS simulations, however, due to the marginal aerodynamic effect of trees on the dispersion of pollutant above canyon (not showed here), the dispersion parameters (A and b) keep nearly constant with the variation of trees. By modifying $\langle C_{\rm L}^* \rangle_{\rm C}$ and ER, the differences between operational model and LES results are controlled under 5% when the deposition velocity is 0 (Fig. 15b). However, when the deposition effect is considerable, the overestimation of OUPM is also noticeable. When the deposition effect is included, $\langle C_{\rm L}^* \rangle_{\rm C}$ decreases compared to the case without deposition with the same LAI (Fig. 9). The deposition effect can be easily associated with normalized canyonaveraged deposition velocity V_d^* . We denote V_d^* in CA1 as $V_{d,L}^*$ and V_d^* in CA2 as $V_{d,B}^*$. When LAI is small, $V_{d,B}^*$ is almost equal to $V_{d,L}^*$, while it increases higher than $V_{d,L}^*$ when LAI is large (Fig. 14b). This might be because the dense canopy results a higher concentration in the pedestrian area (Fig. 6), while the LAD is 0 in this region (Fig. 2). Here, we use $V_{d,B}^*$ to evaluate the deposition effect of vegetation on the ER and the transport of plume above the canopy. The deposition effect results in a reduction of ER with an increase in LAI (Fig. 14a). By introducing

516

517

518

519

520

521

522

523

524

525

526

527

528

529

530

531

532

533

534

535

536

537

538

539

540

541

a flux exchange coefficient γ , the exchange rate in the presence of deposition (denoted by ER_{dep}) can

be related to $\langle V_d^* \rangle$ and to the ER without deposition (denoted by ER₀):

$$ER_{dep} = \frac{1}{1 + \gamma V_{dB}^*} ER_0.$$
 (23)

- 543 $\gamma \sim (\sqrt{2}\pi)/\sigma_{w,R}$ according to Soulhac et al. (2011), and γ is approximated to 3.0 in this study. Fig. 14
- 544 (a) shows that Eq. (23) works well to predict ER_{dep} . Detailed deducing process is posted in
- 545 Supplementary.
- Further, the deposition should also be considered when calculating the background concentration
- $\langle C_{\rm B}^* \rangle_{\rm R}^{}(n)$. The deposition can be treated as negative sources if the deposition flux can be determined.
- 548 For ENDLESS model, however, a solution of advection-diffusion equation with constant deposition
- velocity V_d on the surface based on a constant eddy-diffusivity assumption can be used to calculate
- 550 $C_1(x', y')$ directly (Smith, 1962; Rao, 1981; Horst, 1984):

551
$$C_{1}(x',z') = \frac{2q}{\sqrt{2\pi}\overline{u}\sigma_{z}} \exp\left(-\frac{z'^{2}}{2\sigma_{z}^{2}}\right) \left[1 - 2\sqrt{2\pi}\frac{V_{d}x'}{\overline{u}\sigma_{z}} \exp\xi^{2} \operatorname{erfc}\xi\right], \tag{24}$$

in which,

$$\xi = \frac{z'}{\sqrt{2}\sigma_z} + \sqrt{2}\frac{V_d x'}{\bar{u}\sigma_z} . \tag{25}$$

- Similarly, we assume $\langle C_1^* \rangle_R (n) = C_1 (2(n-1)w_b, 0)u_r h/q$ and Eqs. (24) and (25) can be
- 555 approximated as

556
$$\left\langle C_{1}^{*}\right\rangle_{R}\left(n\right) = \frac{\sqrt{2/\pi}}{\overline{u}^{*}\sigma_{-}^{*}} \left[1 - 2\sqrt{\pi}\xi^{*}\exp\left(\xi^{*2}\right)\operatorname{erfc}\left(\xi^{*}\right)\right] \text{ and }$$
 (26)

$$\xi^* = \frac{\sqrt{2} \left(n - 1 \right) V_{d,B}^*}{\overline{u}^* \sigma_z^*}$$

- More detailed deducing process can be found in Supplement. If $V_{d,B}^* = 0$, the solution Eq. (26) can be
- reduced to the Gaussian plume model Eq. (20).
- Finally, the RE can reduce to under 5% for all cases after introducing canyon deposition velocity
- 562 $V_{d,B}^*$ and modifying $\langle C_L^* \rangle_C$ and ER (Fig. 15c). This suggests that the OUPM can be a good tool to

predict pollution even when the vegetation effect is included. Nevertheless, parameterization is needed for more complex and realistic situations in the future.

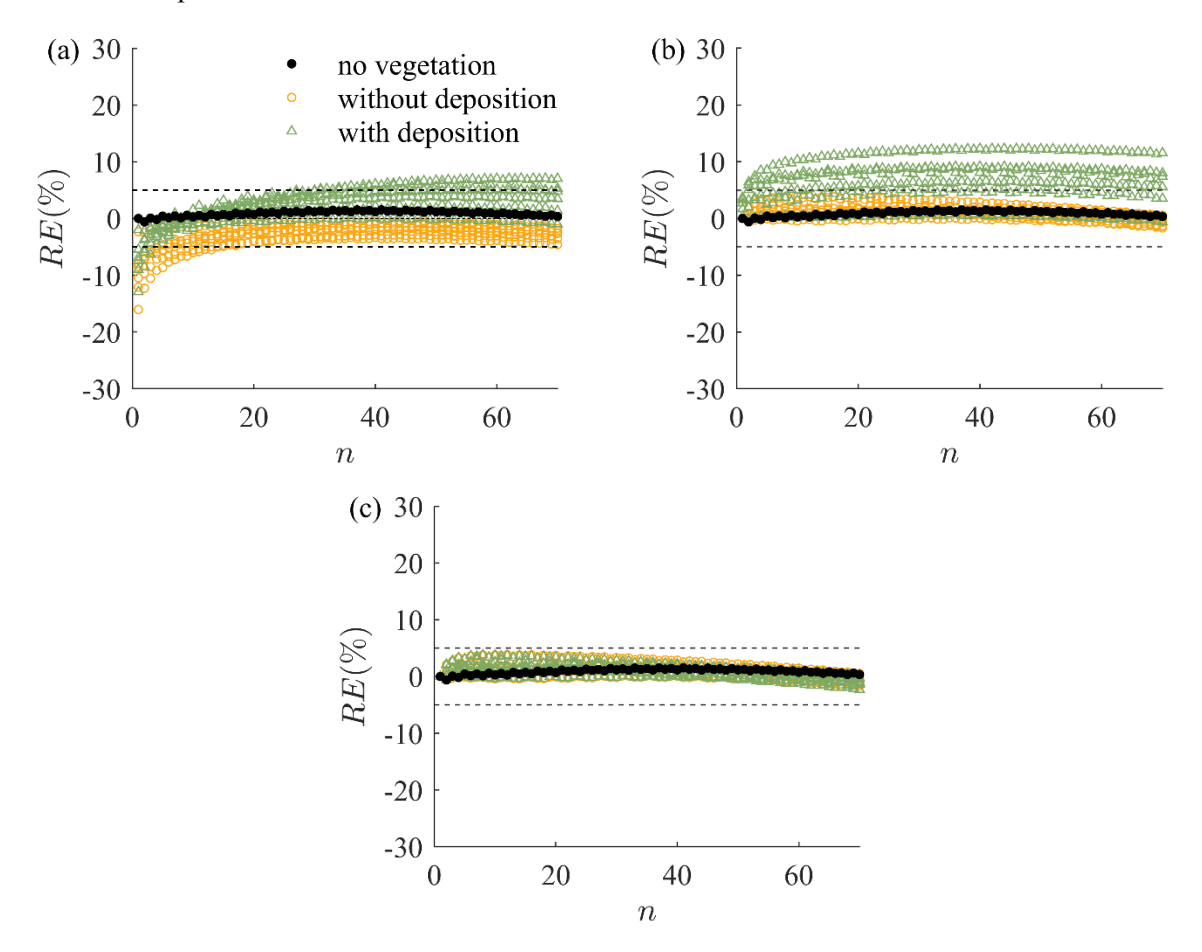


Fig. 15 (Color online) The relative error between the canyon-averaged concentration computed by OUPM and LES: (a) OUPM without trees, (b) OUPM with aerodynamic effect of trees, and (c) OUPM with both aerodynamic and deposition effects of trees. Dashed lines indicate an error of 5%.

4. Conclusions

In this study, LES were performed using ENDLESS to evaluate the effect of street trees on air quality under different emission scenarios and at different scales. For local emissions, increasing vegetation reduces flow within the canyon, increasing concentrations in the vicinity of the leeward wall and reducing concentrations in the windward wall. The deposition effects are smaller than aerodynamic effects. On the other hand, vegetation has almost no effect on the transport of background pollution into the canyon or its distribution within the canyon, which tend to be uniform. However, when a sequence

of canyons is used to investigate the neighborhood scale problem, vegetation works as a particle sink has a large impact in reducing the rate of increase of background pollution with distance from the urban edge. Thus, we conclude that the two effects of vegetation usually mentioned in the literature work at different spatial scales: while reduced ventilation has clear detrimental effects at the canyon scale, the deposition (or filtration effect) has beneficial effects that only manifest in a considerable way at a larger scale. Consequently, an assessment of the true effect of trees on air quality must consider these two distinct spatial scales. Our results suggest that for pollutants with large deposition velocities (such as particles with a diameter smaller than 30 nm or larger than $10 \mu m$), the presence of vegetation is predominantly beneficial at urban scales, especially for areas with much lower local pollution than background transport pollution. Meanwhile, for small deposition velocities, the presence of vegetation is negligible at these large scales. The reduced ventilation is problematic only for the first few dozen canyons where concentration patterns are dominated by local sources.

In addition, this study investigates the aerodynamic and deposition effect of trees on the establishment of the OUPM. Results show that the aerodynamic effect contributes to an increase in concentration from local emissions and a decrease in the ER of background pollution into the canyon. The introduction of canyon-averaged deposition velocity can describe the deposition effect well. With these modifications, the predictions of OUPM show good agreement with the LES results, which suggests that OUPM can be an efficient and economic tool for investigating urban air quality, even for more complex canopies.

In this study, we did not attempt to cover the large parameter space needed to fully characterize the effects of trees on PM2.5 in urban environments. Results are expected to depend on urban geometry and configuration, meteorological conditions, particle size and emission, and vegetation characteristics and distribution within the urban environment. Clearly, a complete exploration of all these effects is challenging, and future research should perhaps focus on identifying the parameters that have a stronger impact on the results. However, it is clear that these future studies should encompass both the canyon and neighborhood scales, and that the ENDLESS approach may be beneficial in exploring these effects.

601

602

603

Acknowledgment

- This research was supported by National Natural Science Foundation of China (NSFC) under grant
- No. 11732008. MC was supported by the National Science Foundation (NSF) grant AGS-1644375.

606

References:

- Abhijith, K. V., P. Kumar, J. Gallagher, A. McNabola, R. Baldauf, F. Pilla, B. Broderick, S. Di Sabatino and B.
- Pulvirenti(2017). "Air pollution abatement performances of green infrastructure in open road and built-up street
- canyon environments--A review." <u>Atmospheric Environment</u> **162**: 71--86.
- Anderson, W., Q. Li and E. Bou-Zeid(2015). "Numerical simulation of flow over urban-like topographies and
- evaluation of turbulence temporal attributes." <u>Journal of Turbulence</u> **16**(9): 809-831.
- Beckett, K. P., P. H. Freer-Smith and G. Taylor(2000). "The capture of particulate pollution by trees at five
- 614 contrasting urban sites." <u>Arboricultural Journal</u> **24**(2-3): 209--230.
- Boppana, V. B. L., Z. T. Xie and I. P. Castro(2014). "Thermal Stratification Effects on Flow Over a Generic Urban
- 616 Canopy." Boundary-Layer Meteorology 153(1): 141-162.
- Brantley, H. L., G. S. Hagler, P. J. Deshmukh and R. W. Baldauf(2014). "Field assessment of the effects of
- roadside vegetation on near-road black carbon and particulate matter." Science of the Total Environment 468: 120-
- 619 -129.
- Britter, R. E. and S. R. Hanna(2003). "Flow and dispersion in urban areas." Annual Review of Fluid Mechanics
- **35**(1): 469-496.
- Brown, M. J., R. E. Lawson, D. S. Decroix and R. L. Lee(2000). Mean Flow and Turbulence Measurement around
- a 2-D Array of Buildings in a Wind Tunnel.
- 624 Buccolieri, R., C. Gromke, S. Di Sabatino and B. Ruck(2009). "Aerodynamic effects of trees on pollutant
- 625 concentration in street canyons." <u>Science of The Total Environment</u> **407**(19): 5247--5256.
- 626 Buccolieri, R., J. L. Santiago, E. Rivas and B. Sánchez(2018). "Review on urban tree modelling in CFD
- 627 simulations: Aerodynamic, deposition and thermal effects." Urban Forestry & Urban Greening 31: 212-220.
- 628 Carruthers, D. J., H. A. Edmunds, A. E. Lester, C. A. McHugh and R. J. Singles(2000). "Use and validation of
- 629 ADMS-Urban in contrasting urban and industrial locations." <u>International Journal of Environment and Pollution</u>
- **14**(1-6): 364--374.
- 631 Cavanagh, J. E., P. Zawar-Reza and J. G. Wilson(2009). "Spatial attenuation of ambient particulate matter air
- pollution within an urbanised native forest patch." <u>Urban Forestry & Urban Greening</u> 8(1): 21--30.
- Chamecki, M., C. Meneveau and M. B. Parlange(2008). "A hybrid spectral/finite-volume algorithm for large-eddy
- simulation of scalars in the atmospheric boundary layer." Boundary-layer meteorology 128(3): 473--484.
- 635 Chen, B., D. Yang, C. Meneveau and M. Chamecki(2016). "ENDLESS: An extended nonperiodic domain large-
- eddy simulation approach for scalar plumes." Ocean Modelling 101: 121-132.
- 637 Chen, B., D. Yang, C. Meneveau and M. Chamecki(2018). "Numerical study of the effects of chemical dispersant
- on oil transport from an idealized underwater blowout." Physical Review Fluids 3(8).

- 639 Chen, M., F. Dai, B. Yang and S. Zhu(2019). "Effects of neighborhood green space on PM2. 5 mitigation:
- Evidence from five megacities in China." <u>Building and Environment.</u>
- 641 Chen, X., T. Pei, Z. Zhou, M. Teng, L. He, M. Luo and X. Liu(2015). "Efficiency differences of roadside greenbelts
- with three configurations in removing coarse particles (PM10): A street scale investigation in Wuhan, China."
- 643 <u>Urban Forestry & Urban Greening</u> **14**(2): 354 360.
- 644 Cheng, W. C., C. H. Liu and D. Y. C. Leung(2008). "Computational formulation for the evaluation of street canyon
- ventilation and pollutant removal performance." Atmospheric Environment **42**(40): 9041-9051.
- 646 Cui, Z., X. Cai and C. J Baker(2004). "Large-eddy simulation of turbulent flow in a street canyon." Quarterly
- Journal of the Royal Meteorological Society **130**(599): 1373--1394.
- Freer-Smith, P. H., A. A. Elkhatib and G. Taylor(2004). "Capture of Particulate Pollution by Trees: A Comparison
- of Species Typical of Semi-Arid Areas (Ficus Nitida and Eucalyptus Globulus) with European and North
- American Species." Water Air & Soil Pollution **155**(1-4): 173-187.
- Freer-Smith, P. H., K. P. Beckett and G. Taylor(2005). "Deposition velocities to Sorbus aria, Acer campestre,
- Populus deltoides X trichocarpa 'Beaupre', Pinus nigra and X Cupressocyparis leylandii for coarse, fine and ultra-
- fine particles in the urban environment." <u>Environmental Pollution</u> **133**(1): 157--167.
- Gaskell, P. H. and A. K. C. Lau(1988). "Curvature-compensated convective transport: {SMART}, A new
- boundedness- preserving transport algorithm." International Journal for Numerical Methods in Fluids 8(6): 617--
- 656 641.
- Giometto, M. G., A. Christen, P. E. Egli, M. F. Schmid, R. T. Tooke, N. C. Coops and M. B. Parlange(2017).
- "Effects of trees on mean wind, turbulence and momentum exchange within and above a real urban environment."
- 659 Advances in Water Resources **106**: 154--168.
- 660 Gromke, C. and B. Ruck(2007). "Influence of trees on the dispersion of pollutants in an urban street canyon—
- Experimental investigation of the flow and concentration field." <u>Atmospheric Environment</u> **41**(16): 3287-3302.
- 662 Gromke, C. and B. Ruck(2012). "Pollutant concentrations in street canyons of different aspect ratio with avenues
- of trees for various wind directions." <u>Boundary-Layer Meteorology</u> **144**(1): 41--64.
- Guo, S., M. Hu, M. L. Zamora, J. Peng, D. Shang, J. Zheng, Z. Du, Z. Wu, M. Shao and L. Zeng(2014).
- "Elucidating severe urban haze formation in China." <u>Proceedings of the National Academy of Sciences of the</u>
- 666 United States of America **111**(49): 17373.
- 667 Hirabayashi, S., C. N. Kroll and D. J. Nowak(2012). "i-Tree eco dry deposition model descriptions." <u>Citeseer</u>.
- Horst, T. W.(1984). The Modification of Plume Models to Account for Dry Deposition, Springer Netherlands.
- Irga, P. J., M. D. Burchett and F. R. Torpy(2015). "Does urban forestry have a quantitative effect on ambient air
- quality in an urban environment?" <u>Atmospheric Environment</u> **120**: 173--181.
- Janhäll, S.(2015). "Review on urban vegetation and particle air pollution--Deposition and dispersion."
- 672 <u>Atmospheric Environment</u> **105**: 130--137.
- Jeanjean, A. P., P. S. Monks and R. J. Leigh(2016). "Modelling the effectiveness of urban trees and grass on PM2.
- 5 reduction via dispersion and deposition at a city scale." Atmospheric environment 147: 1--10.
- Jeanjean, A. P., R. Buccolieri, J. Eddy, P. S. Monks and R. J. Leigh(2017). "Air quality affected by trees in real
- street canyons: The case of Marylebone neighbourhood in central London." <u>Urban Forestry & Urban Greening</u> 22:
- 677 41--53.
- Jin, S., J. Guo, S. Wheeler, L. Kan and S. Che(2014). "Evaluation of impacts of trees on PM2.5 dispersion in urban
- streets." <u>Atmospheric Environment</u> **99**: 277--287.
- Karjalainen, P., L. Pirjola, J. Heikkilä, T. Lähde, T. Tzamkiozis, L. Ntziachristos, J. Keskinen and T.
- Rönkkö(2014). "Exhaust particles of modern gasoline vehicles: A laboratory and an on-road study." Atmospheric
- 682 Environment 97: 262--270.

- Katul, G. G., T. G. O. Nholm, S. Launiainen and T. Vesala(2011). "The effects of the canopy medium on dry
- deposition velocities of aerosol particles in the canopy sub-layer above forested ecosystems." Atmospheric
- 685 <u>Environment</u> **45**(5): 1203--1212.
- 686 Li, Q. and Z. Wang(2018). "Large-eddy simulation of the impact of urban trees on momentum and heat fluxes."
- Agricultural and Forest Meteorology **255**: 44--56.
- 688 Li, Q., E. Bou-Zeid and W. Anderson(2016). "The impact and treatment of the Gibbs phenomenon in immersed
- boundary method simulations of momentum and scalar transport." <u>Journal of Computational Physics</u> 310: 237--
- 690 251.
- 691 Lin, X., M. Chamecki, G. Katul and X. Yu(2018). "Effects of leaf area index and density on ultrafine particle
- deposition onto forest canopies: A {LES} study." <u>Atmospheric Environment</u> **189**: 153--163.
- 693 Lovett, G. M.(1994). "Atmospheric Deposition of Nutrients and Pollutants in North America: An Ecological
- Perspective." <u>Ecological Applications</u> **4**(4): 629--650.
- Maricq, M. M., D. H. P. And and R. E. Chase(1999). "Gasoline Vehicle Particle Size Distributions: Comparison
- of Steady State, FTP, and US06 Measurements." Environmental Science & Technology 33(12): 2007-2015.
- McHugh, C. A., D. J. Carruthers and H. A. Edmunds(1997). "ADMS-Urban: an air quality management system
- 698 for traffic, domestic and industrial pollution." International Journal of Environment & Pollution 8(3-4): 666-674.
- Meroney, R. N., M. Pavageau, S. Rafailidis and M. Schatzmann (1996). "Study of line source characteristics for 2-
- D physical modelling of pollutant dispersion in street canyons." <u>Journal of Wind Engineering and Industrial</u>
- 701 <u>Aerodynamics</u> **62**(1): 37--56.
- 702 Michioka, T., H. Takimoto, H. Ono and A. Sato(2016). "Effect of Fetch on a Mechanism for Pollutant Removal
- from a Two-Dimensional Street Canyon." <u>Boundary-Layer Meteorology</u> **160**(1): 185-199.
- Moonen, P., C. Gromke and V. Dorer(2013). "Performance assessment of Large Eddy Simulation (LES) for
- modeling dispersion in an urban street canyon with tree planting." Atmospheric environment 75: 66--76.
- Namdeo, A. K. and J. J. Colls(1996). "Development and evaluation of SBLINE, a suite of models for the prediction
- of pollution concentrations from vehicles in urban areas." <u>Science of the total environment</u> **189**: 311--320.
- Nieuwstadt, F. T. M., P. J. Mason, C. H. Moeng and U. Schumann(1993). Large-Eddy Simulation of the
- 709 <u>Convective Boundary Layer: A Comparison of Four Computer Codes</u>, Springer Berlin Heidelberg.
- 710 Oke, T. R.(1988). "Street design and urban canopy layer climate." Energy and buildings 11(1-3): 103--113.
- Pan, Y., M. Chamecki and S. A. Isard(2014). "Large-eddy simulation of turbulence and particle dispersion inside
- 712 the canopy roughness sublayer." <u>Journal of Fluid Mechanics</u> **753**: 499--534.
- Pavageau, M.(1996). "Concentration fluctuations in urban street canyons groundwork for future studies."
- 714 <u>Meteorological Institute of the University of Hamburg Tech. Rep.</u>
- Pavageau, M. and M. Schatzmann(1999). "Wind tunnel measurements of concentration fluctuations in an urban
- street canyon." Atmospheric Environment 33(24-25): 3961--3971.
- 717 Petroff, A., A. Mailliat, M. Amielh and F. Anselmet(2008). "Aerosol dry deposition on vegetative canopies. Part
- 718 I: Review of present knowledge." <u>Atmospheric Environment</u> **42**(16): 3625--3653.
- Pope, C. A., R. T. Burnett, M. J. Thun, E. E. Calle, D. Krewski, K. Ito and G. D. Thurston(2002). "Lung cancer,
- 720 cardiopulmonary mortality, and long-term exposure to fine particulate air pollution." Jama-Journal of the
- 721 <u>American Medical Association</u> **287**(9): 1132-1141.
- Pöschl, U.(2005). "Atmospheric aerosols: composition, transformation, climate and health effects." Angewandte
- 723 <u>Chemie International Edition</u> **44**(46): 7520--7540.
- Rao, K. S. M. X.(1981). <u>Analytical solutions of a gradient-transfer model for plume deposition and sedimentation</u>,
- 725 US Department of Commerce, National Oceanic and Atmospheric Administration, Environmental Research
- 726 Laboratories.

- Ries, K. and J. Eichhorn(2001). "Simulation of effects of vegetation on the dispersion of pollutants in street
- 728 canyons." Meteorologische Zeitschrift 10(4): 229--233.
- Righi, S., P. Lucialli and E. Pollini(2009). "Statistical and diagnostic evaluation of the ADMS-Urban model
- compared with an urban air quality monitoring network." <u>Atmospheric Environment</u> **43**(25): 3850 3857.
- Roupsard, P., M. Amielh, D. Maro, A. Coppalle, H. Branger, O. Connan, P. Laguionie, D. Hébert and M.
- 732 Talbaut(2013). "Measurement in a wind tunnel of dry deposition velocities of submicron aerosol with associated
- turbulence onto rough and smooth urban surfaces." Journal of Aerosol Science 55(1): 12-24.
- Salem, N. B., V. Garbero, P. Salizzoni, G. Lamaison and L. Soulhac(2015). "{Modelling Pollutant Dispersion in
- a Street Network." Boundary-Layer Meteorology **155**(1): 157-187.
- Salim, S. M., S. C. Cheah and A. Chan(2011). "Numerical simulation of dispersion in urban street canyons with
- avenue-like tree plantings: Comparison between RANS and LES." <u>Building & Environment</u> **46**(9): 1735-1746.
- 738 Santiago, J., A. Martilli and F. Martin(2017). "On dry deposition modelling of atmospheric pollutants on
- vegetation at the microscale: Application to the impact of street vegetation on air quality." Boundary-layer
- 740 meteorology **162**(3): 451--474.
- Setala, H., V. Viippola, A. Rantalainen, A. Pennanen and V. Yli-Pelkonen(2013). "Does urban vegetation mitigate
- air pollution in northern conditions?" Environmental Pollution **183**(SI): 104-112.
- 743 Shaw, R. H. and U. Schumann(1992). "Large-eddy simulation of turbulent flow above and within a forest."
- 744 <u>Boundary-Layer Meteorology</u> **61**(1-2): 47--64.
- Smith, F. B.(1962). "The Problem of Deposition in Atmospheric Diffusion of Particulate Matter." <u>Journal of the</u>
- 746 <u>Atmospheric Sciences</u> **19**(5): 429-433.
- Soulhac, L., P. Salizzoni, F. X. Cierco and R. Perkins(2011). "The model SIRANE for atmospheric urban pollutant
- dispersion; part I, presentation of the model." Atmospheric Environment **45**(39): 7379-7395.
- Soulhac, L., P. Salizzoni, P. Mejean, D. Didier and I. Rios(2012). "The model SIRANE for atmospheric urban
- 750 pollutant dispersion; PART II, validation of the model on a real case study." Atmospheric Environment 49: 320 -
- 751 337.
- 752 Teske, M. E. and H. W. Thistle(2004). "A library of forest canopy structure for use in interception modeling."
- 753 Forest Ecology and Management **198**(1-3): 341--350.
- Tseng, Y. H. and J. H. Ferziger(2003). "A ghost-cell immersed boundary method for flow in complex geometry."
- 755 <u>Journal of Computational Physics</u> **192**(2): 593-623.
- Vos, P. E. J., B. Maiheu, J. Vankerkom and S. Janssen (2013). "Improving local air quality in cities: To tree or not
- 757 to tree?" Environmental Pollution **183**: 113--122.
- Vranckx, S., P. Vos, B. Maiheu and S. Janssen(2015). "Impact of trees on pollutant dispersion in street canyons:
- A numerical study of the annual average effects in Antwerp, Belgium." <u>Science of The Total Environment</u> **532**:
- 760 474 483.
- Wang, C., Q. Li and Z. Wang(2018). "Quantifying the impact of urban trees on passive pollutant dispersion using
- a coupled large-eddy simulation-Lagrangian stochastic model." <u>Building and Environment</u> **145**: 33--49.
- Wong, C. C. and C. Liu(2013). "Pollutant plume dispersion in the atmospheric boundary layer over idealized urban
- roughness." Boundary-layer meteorology **147**(2): 281--300.
- Xie, X., C. Liu, D. Y. C. Leung and M. K. H. Leung(2006). "Characteristics of air exchange in a street canyon
- with ground heating." Atmospheric Environment **40**(33): 6396--6409.
- Xue, F. and X. Li(2017). "The impact of roadside trees on traffic released {PM} 10 in urban street canyon:
- Aerodynamic and deposition effects." <u>Sustainable Cities and Society</u> **30**: 195--204.
- 769 Yin, S., Z. Shen, P. Zhou, X. Zou, S. Che and W. Wang(2011). "Quantifying air pollution attenuation within urban
- parks: An experimental approach in Shanghai, China." Environmental Pollution 159(8-9SI): 2155-2163.

- 771 Yli-Pelkonen, V., H. Set A L A and V. Viippola(2017). "Urban forests near roads do not reduce gaseous air
- pollutant concentrations but have an impact on particles levels." <u>Landscape and Urban Planning</u> **158**: 39--47.
- Zhao, X. J., P. S. Zhao, J. Xu, W. Meng, W. W. Pu, F. Dong, D. He and Q. F. Shi(2013). "Analysis of a winter
- 774 regional haze event and its formation mechanism in the North China Plain." <u>Atmospheric Chemistry and Physics</u>
- 775 **13**(11): 5685--5696.
- 776 Zhu, Y., W. C. Hinds, S. Kim and C. Sioutas(2002). "Concentration and Size Distribution of Ultrafine Particles
- Near a Major Highway." <u>Journal of the Air & Waste Management Association</u> **52**(9): 1032-1042.